Slow Solvation Dynamics at the Active Site of an Enzyme: Implications for Catalysis†

Soumi Guha,‡ Kalyanasis Sahu,§ Durba Roy,§ Sudip Kumar Mondal,§ Siddhartha Roy,*,‡,|| and Kankan Bhattacharyya*,§

Department of Biophysics, Bose Institute, P-1/12 CIT Scheme VIIM, Kolkata 700 054, India, Physical Chemistry Department, Indian Association for the Cultivation of Science, Jadavpur, Kolkata 700 032, India, and Indian Institute of Chemical Biology, Jadavpur, Kolkata 700 032, India

Received December 13, 2004; Revised Manuscript Received February 28, 2005

ABSTRACT: Solvation dynamics at the active site of an enzyme, glutaminyl-tRNA synthetase (GlnRS), was studied using a fluorescence probe, acrylodan, site-specifically attached at cysteine residue C229, near the active site. The picosecond time-dependent fluorescence Stokes shift indicates slow solvation dynamics at the active site of the enzyme, in the absence of any substrate. The solvation dynamics becomes still slower when the substrate (glutamine or $tRNA^{Gln}$) binds to the enzyme. A mutant Y211H-GlnRS was constructed in which the glutamine binding site is disrupted. The mutant Y211H-GlnRS labeled at C229 with acrylodan exhibited significantly different solvent relaxation, thus demonstrating that the slow dynamics is indeed associated with the active site. Implications for catalysis and specificity have been discussed.

A long-standing but yet unattained goal in enzymology is to elucidate the origin of large rate enhancement and substrate specificity (molecular recognition) of an enzyme. Many factors may contribute to the extraordinary rate enhancement and substrate specificity. Several recent computer simulation and theoretical studies (*1*−*3*) have stressed the importance of preorganization of the active site and by implication the associated water molecules. It is proposed that at the active site of an enzyme the water molecules and other polar residues are already optimally organized specifically for the transition state of the catalyzed reaction (*1*−*6*). The natural question is what happens to these preorganized active sites when a polar species approaches or when a dipole is created suddenly in the immediate vicinity. If under the influence of an external charge the water molecules and side chains reorganize too fast, the structure of the active site may be seriously disturbed, and this may impair the biological activity. It is thus of fundamental importance to study the solvation dynamics at the active site of an enzyme.

Dynamics of the water molecules in the vicinity of a protein has been studied using a variety of experimental techniques such as inelastic neutron scattering (*7*), NMR (*8*, *9*), and, most recently, ultrafast laser spectroscopy (*10*−*21*). The experimental studies are supplemented by an analytic theoretical model (*22*), and computer simulations on proteins (*23*, *24*), other organized assemblies (*25*−*29*), and water surface (*30*). According to these studies, a vast majority of the water molecules near a protein remain almost as fast as those in bulk water. However, a small fraction (5−20%) of the buried water molecules are found to be 100−1000 times slower. For instance, according to NMR (*8*, *9*) and simulations (*23*, *24*) in bulk water, the residence time of a water molecule is ∼5 ps, while at the surface of a protein (lysozyme), the residence time is 5−7 times longer (*23*). However, according to simulations (*23*, *24*) for the same protein (lysozyme), the residence time of the buried water molecules is 1000 times longer (*22*, *23*). In bulk water, solvation dynamics occurs with a major sub-picosecond component and a minor component of ∼1 ps (*31*−*34*). However, Fleming and co-workers detected a small (8%) component of 530 ps for a noncovalent probe (eosin) bound to lysozyme (*10*). Zewail and co-workers (*14*) used tryptophan as an intrinsic solvation probe and detected a component of 40−50 ps. We have earlier reported that the solvation dynamics of a probe in a protein glutaminyl-tRNA synthetase (GlnRS)[1] is location-dependent. For a probe covalently attached at the surface of GlnRS, we detected a fast solvation time of 120 ps (*20*). For the same protein, a noncovalent probe which goes deep inside the protein exhibits a solvation time of 1400 ps (*19*). In this work, we report on solvation dynamics of a fluorescence probe (acrylodan) covalently attached very close to the active site of GlnRS.

† We thank the Department of Science and Technology (DST) and the Council of Scientific and Industrial Research (CSIR), Government of India, for generous support. We also thank CSIR for fellowships to S.G., D.R., S.K.M., and K.S.

* To whom correspondence should be addressed. S.R.: e-mail, sidroy@vsnl.com; fax, (91)-33-2334-3886; phone, (91)-33-2473-3491. K.B.: e-mail, pckb@mahendra.iacs.res.in; fax, (91)-33-2473-2805; phone, (91)-33-2473-3542.

‡ Bose Institute.

§ Indian Association for the Cultivation of Science.

|| Indian Institute of Chemical Biology.

[1] Abbreviations: GlnRS, glutaminyl-tRNA synthetase; C229, cysteine 229; DTBN, 5,5′-dithiobis(2-nitrobenzoic acid); TAP, thioaminophthalimide; TDFSS, time-dependent fluorescence Stokes shift; TRES, time-resolved emission spectra; CD, circular dichroism; PRODAN, 6-propionyl-2-(*N*,*N*-dimethylamino)naphthalene.

10.1021/bi0473915 CCC: $30.25
Published on Web 05/28/2005

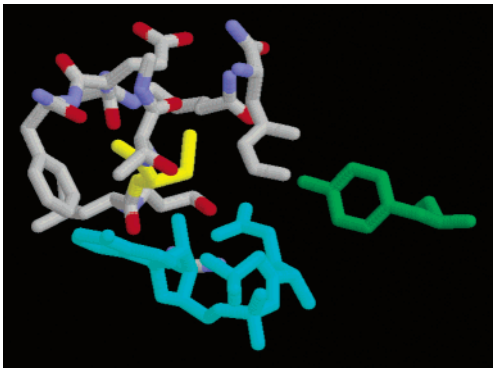

FIGURE 1: Depiction of residues within 5−6 Å of C229 of GlnRS. PDB entry 1QTQ was used. The figures were generated using Rasmol. The yellow residue is C229, the green residue Y211, and the cyan molecule a transition-state analogue containing AMP and glutamine.

The biological function of GlnRS is to acylate the tRNA that is specific for glutamine ($tRNA^{gln}$) with the amino acid glutamine for protein synthesis. Very recently, detailed structural information for GlnRS in the free form and bound to various ligands (e.g., glutamine and $tRNA^{gln}$) has been obtained using high-resolution X-ray crystallography (*35*). Figure 1 shows a part of the crystal structure of GlnRS around the active site. i.e., glutamine binding pocket. Figure 2 shows crystal structures of the active site of GlnRS in the free protein and enzyme−substrate complex. The crystal structure of GlnRS reveals the presence of a large number of water molecules in both the free protein and the enzyme−substrate complex (*35*). GlnRS contains eight half-cysteines and one disulfide. Of them, cysteine 229 (C229) is located very close to the active site of GlnRS. The −SH group of C229 is 4.2 Å from amide group of substrate glutamine and 5.6 Å from the hydroxyl group of the tyrosine residue (Y211) which forms a hydrogen bond with glutamine (*35*−*37*). Mutation or modification (e.g., labeling with acrylodan, etc.) of C229 does not significantly influence the catalytic activity of GlnRS (*38*, *39*). Thus, C229, though very close to the active site, is not directly involved in biological activity. Thus, one can study solvation dynamics at the active site of GlnRS without destroying the catalytic activity by labeling GlnRS at C229 with acrylodan (Scheme 1).

In the first part of this work, we will establish that C229 is the most reactive sulfhydryl group of GlnRS and is the site which is labeled with acrylodan. Perona and co-workers (*36*) previously studied the reactivity of various cysteines of GlnRS toward heavy atom (Au, Hg, etc.) reagents. From a detailed analysis of the kinetics of the reaction between 5,5′-dithiobis(2-nitrobenzoic acid) (DTNB) and GlnRS in solution, we have detected three types of reactive sulfhydryl groups of GlnRS (*38*, *39*). In this work, we will show that C229 is the most reactive sulfhydryl group and the most probable site where acrylodan reacts.

After establishing the location of the acrylodan, we report on the solvation dynamics in wild-type GlnRS and also in GlnRS bound to glutamine, $tRNA^{gln}$, and ATP. To study solvation dynamics, we use the time-dependent fluorescence Stokes shift technique. Finally, we study solvation dynamics in a mutant GlnRS in which the glutamine binding pocket is disrupted.

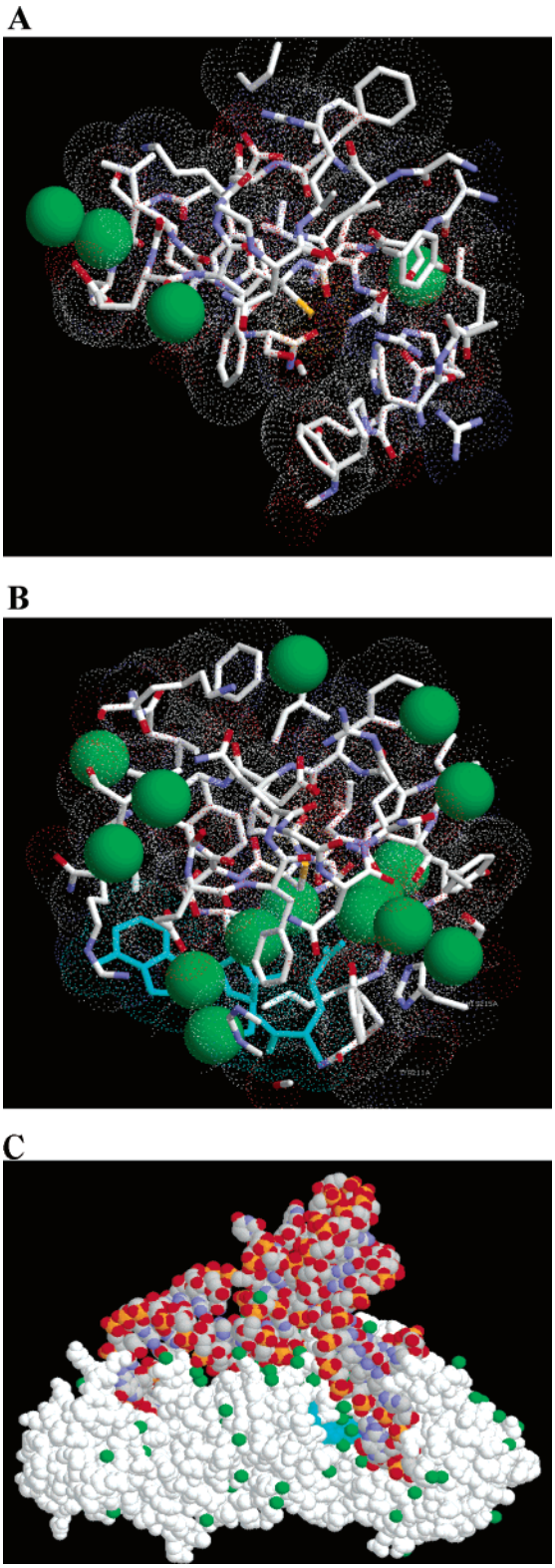

FIGURE 2: Crystal structures (*35*) of the active site of glutaminyl-tRNA synthetase (A) in unliganded form and (B) in complex with $tRNA^{gln}$, $AMPCH_2PP$, and glutamine. C229 is in the middle with a yellow side chain for the sulfur. Structures within 1.2 nm of C229 are shown. The orientations are approximately the same. The tRNA chain is omitted for clarity in panel B. The green spheres are the water molecules, and the cyan structures are glutamine and $AMPCH_2PP$ in panel B. PDB entries 1NYL (A) and 1O0B (B) were used. The figures were generated using RasTop 2.0.3. (C) Full crystal structure of the complex (PDB entry 1O0B).

Scheme 1: (a) Acrylodan (**I**) Labeling of a −SH Group of a Protein and (b) Structure of PRODAN (**II**)

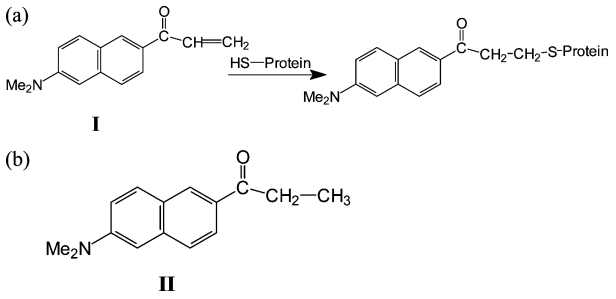

EXPERIMENTAL PROCEDURES

Methods of purification of GlnRS and $tRNA^{gln}$ and also labeling of GlnRS with acrylodan and DTNB have been described in detail in our earlier publications (*38*, *39*). In all our spectroscopic studies, we used a 0.1 M Tris-HCl buffer (pH 7.5) containing 15 mM $MgCl_2$. The concentrations of the components were as follows: 6.4 μM GlnRS and, when added, 6.4 μM $tRNA^{gln}$, 2 mM L-glutamine, and 2.5 mM ATP. In the case of Y211H-GlnRS, the protein concentration was 4.4 μM.

Y211H and C229G site-directed mutants of GlnRS were made via the PCR-based overlap extension procedure (*17*) using two mutagenic primers and outside primers with EcoRI and BamHI restriction sites and high-fidelity Pfu polymerase. The total mutant gene was sequenced. The mutagenic primers for Y211H were 5′-TCTACCCGATGCATGACTTCAC-CCAC-3′ and 5′-GTGGGTGAAGTCATGCATCGGGTA-GAT-3′, and those for C229G were 5′-ACGCACTCTCT-GGGCACGCTT-GAGTTC-3′ and 5′-GAACTCAAGCG-TGCCCAGAGAGTGCGT-3′. The forward primer was 5′-CGGAATTCCGAGGAATCCACGATGAGTGAGGCA-3′, and the reverse primer was 5′-GTTCCTTGCCGGATC-CGACGTAAAGCCCCCA-3′.

The mutant gene was initially cloned into the pGEM3z cloning vector and then subcloned into the pthioHisC expression vector containing an affinity tag. The total mutant gene was sequenced. The plasmid encoding the mutant protein was transformed in BL21(DE3) cells. The transformed cells were grown in Luria broth containing 100 μg/mL ampicillin until the absorbance at 595 nm (A_{595}) reached 0.5. Then the cells were induced with 0.5 mM IPTG and grown for an additional 3 h. The harvested cells were resuspended in 50 mM Tris-HCl (pH 7.5) containing 10% glycerol and 2 mM imidazole and lysed by sonication. To the lysates was added 500 mM NaCl, and the mixture was allowed to sit on ice for 30 min. Then the cell debris was removed by centrifugation at 14 000 rpm for 1 h. The clarified supernatant was loaded onto Ni−NTA agarose equilibrated with 50 mM Tris-HCl buffer (pH 7.5) containing 10% glycerol, 500 mM NaCl, and 2 mM imidazole. The column was washed subsequently with 25 mM Tris-HCl buffer (pH 7.5) containing 10% glycerol, 2 mM imidazole, and 200 mM NaCl. The washing flow through was dialyzed extensively against 10 mM KP (pH 7.2) containing 10% glycerol and 20 mM 2-mercaptoethanol. The protein was loaded onto DEAE-cellulose pre-equilibrated with 20 mM phosphate buffer (pH 7.2) containing 10% glycerol and 20 mM 2-mercaptoethanol. The column was washed with 2 column volumes of equilibration buffer and eluted with a phosphate buffer gradient from 20 mM phosphate buffer (pH 7.2) containing 10% glycerol and 20 mM 2-mercaptoethanol to 250 mM phosphate buffer (pH 6.5) containing 10% glycerol and 20 mM 2-mercaptoethanol. The fractions containing the fusion proteins were dialyzed against 20 mM Tris-HCl buffer (pH 8) containing 50 mM NaCl and 2 mM $CaCl_2$ and then incubated with enterokinase to cleave the affinity tag (1:30, w/w) at 23 °C. The reaction mixture was then passed through trypsin−inhibitor agarose and Ni−NTA agarose to remove the cleaved His tag and enterokinase, and the flow through after the two columns contained the purified protein. Both the columns were equilibrated with 20 mM Tris-HCl buffer (pH 8) containing 50 mM NaCl. The purified proteins were finally dialyzed against 20 mM phosphate buffer (pH 7.2) containing 10% glycerol and 20 mM 2-mercaptoethanol and stored at −60 °C.

Steady-state fluorescence spectra were recorded with a Perkin-Elmer MPF 44B spectrofluorimeter. DTNB kinetics was monitored with a Shimadzu UV-160 spectrophotometer at 412 nm. To record fluorescence decays, the samples were excited with a picosecond diode at 405 nm (IBH NanoLED-01), and the emission decays were recorded at magic angle polarization using a Hamamatsu MCP-PMT apparatus (2809U). The time-correlated single-photon counting setup consists of an ORTEC 935 CFD and PCA3 card as a multichannel analyzer. The fluorescence decays were deconvoluted using PTI global lifetime analysis software. The time resolution (instrument response function) of our setup was ∼100 ps. For fluorescence anisotropy decay, emissions at parallel ($I_{||}$) and perpendicular ($I_{\perp}$) polarizations were collected by rotating the analyzer at regular intervals. The anisotropy function $r(t)$ is defined as

$$r(t) = \frac{I_{||}(t) - GI_{\perp}(t)}{I_{||}(t) + 2GI_{\perp}(t)} \quad (1)$$

The G value of the setup was determined using a probe whose rotational relaxation time is very fast, e.g., nile red in methanol.

Circular dichroism spectra were recorded at 25 °C in a JASCO J-600 spectropolarimeter in a cuvette with a path length of 1 mm. The protein concentration of both the wild-type and mutant GlnRS was 2 μM in 0.1 M Tris-HCl buffer (pH 7.5) containing 0.1 M KCl.

For the study of acrylamide quenching, a 2 M stock acrylamide solution was prepared in 0.1 M potassium phosphate buffer (pH 8) containing 0.1 M potassium chloride and 0.1 mM EDTA. Then to a 2 μM protein solution in the same buffer was added a stock acrylamide solution at an interval of 10 to a final concentration of 185 mM. At each acrylamide concentration, fluorescence intensity was measured. The observed fluorescence was corrected for the inner-filter effect using the formula

$$F_{corr} = F_{obs}\,\text{antilog}[(A_{ex} + A_{em})L/2] \quad (2)$$

where L is the path length of the cuvette, the A terms are the absorbances at the excitation and emission wavelengths, and the F values are the corrected and observed fluorescence intensities. The excitation wavelength was 295 nm and the emission wavelength 341 nm. The data were fitted to the Stern−Volmer equation.

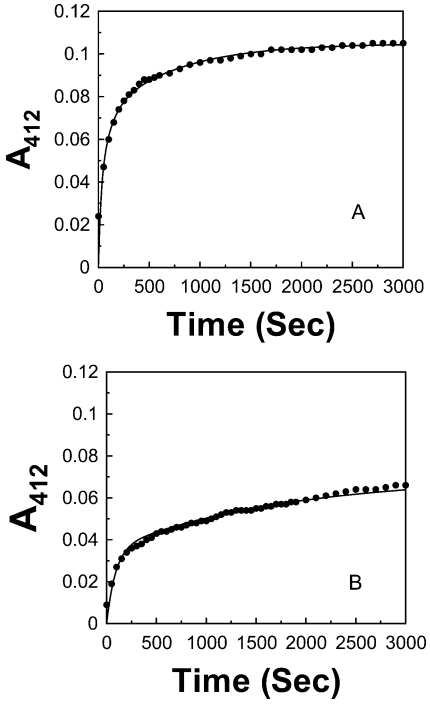

FIGURE 3: Kinetics of the reaction of DTNB with (A) wild-type GlnRS and (B) C229G-GlnRS. Protein concentrations in both cases were 2.66 μM. Solution conditions are described in the text.

RESULTS

Identification of C229 as the Most Reactive Sulfhydryl Group. Previously (*38*, *39*), we had observed one very rapidly reacting sulfhydryl residue which was predominantly modified by acrylodan. Cyanide cleavage of the TNB adduct and mass spectrometry indicated the reactive residue to be C229 (data not shown). To confirm that C229 is indeed the most reactive residue, we have constructed a site-directed mutant where cysteine 229 is replaced with glycine using the overlap extension procedure. The mutant protein (C229G-GlnRS) was purified and exhibited full biological activity in the aminoacylation assay. Figure 3 shows the kinetics of the reaction of DTNB with wild-type GlnRS (Figure 3A) and mutant C229G-GlnRS (Figure 3B). The data were fitted to a biexponential function: $A_0[2 - \exp(-k_1t) - \exp(-k_2t)]$ with time constants ($1/k_1$ and $1/k_2$) of 1.5 and 29 min, respectively. The total absorbance change is consistent with two reactive sulfhydryl groups. Under similar conditions, reactions of wild-type GlnRS could be fitted to a very rapidly reacting SH whose reaction is over within the mixing time and two slower reacting SHs with time constants of 2 and 26 min (Figure 3). This suggests the presence of one very fast and two slower reacting sulfhydryl groups in wild-type GlnRS (*38*, *39*). It is apparent that the extremely rapidly reacting sulfhydryl is absent in the mutant protein C229G-GlnRS, while the rate constants of the other two sulfhydryl groups of the mutant match well with those of the wild-type enzyme. The absence of the very fast component in the mutant protein (which is devoid of cysteine 229) indicates the most reactive cysteine of GlnRS is indeed C229. We have previously shown that acrylodan labeling of wild-type GlnRS causes the disappearance of the fastest reacting sulfhydryl, and only one acrylodan is attached per molecule of GlnRS (*38*, *39*). From this, we conclude that the solvation probe, acrylodan, is bound to the most reactive cysteine, i.e., C229.

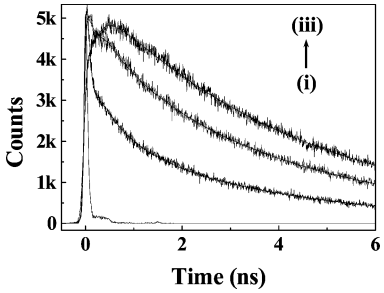

FIGURE 4: Initial portions of the fluorescence decays of acrylodan-labeled GlnRS at (i) 430, (ii) 470, and (iii) 570 nm.

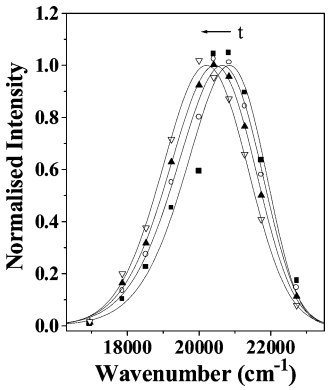

FIGURE 5: Time-resolved emission spectra of acrylodan-labeled GlnRS SDS at 0 (■), 300 (○), 1000 (▲), and 10 000 ps (▽).

Solvation Dynamics of Acrylodan-Labeled Wild-Type GlnRS. To monitor solvation (hydration) dynamics, we have used the time-dependent fluorescence stokes shift (TDFSS) of GlnRS, site-specifically labeled with acrylodan at residue C229. Figure 5 displays fluorescence decays of acrylodan-labeled GlnRS. It is readily seen that at the blue end (440 nm) of the emission spectra of acrylodan, there is a decay with time constants of 750 and 4000 ps, and at the red end (590 nm), a rise of 400 ps precedes the decay with a time constant of 4500 ps. Such a decay at the blue end and the growth at the red end are clear signatures of solvation dynamics. The time-resolved emission spectra (TRES, Figure 4) were constructed using the steady-state emission spectrum, and the parameters of fluorescence decay and the TRES were fitted to a log-normal function as described previously (*41*, *42*). Solvation dynamics is monitored by following the decay of the solvent correlation function $C(t)$ which is defined as (*42*)

$$C(t) = \frac{\nu(t) - \nu(\infty)}{\nu(0) - \nu(\infty)} \tag{3}$$

where $\nu(0)$, $\nu(t)$, and $\nu(\infty)$ denote the observed emission energies (frequencies) at time zero, t, and infinity, respectively. Obviously, in a picosecond setup, a significant portion of the dynamic solvent shift is missed. The emission frequency at time zero, $\nu^{p}_{em}(0)$, may be calculated using the absorption frequency (ν^{p}_{abs}) in a polar medium (i.e., probe bound to GlnRS), using the following relation (*43*)

$$\nu^{p}_{em}(0) = \nu^{p}_{abs} - (\nu^{np}_{abs} - \nu^{np}_{em}) \tag{4}$$

Table 1: Decay Parameters of Solvent Relaxation of Acrylodan-Labeled Wild-Type and Mutant Glutaminyl-tRNA Synthetases

system	$\Delta\nu^a$ (cm^{-1})	a_1	$\tau_1{}^{b,c}$ (ps)	a_2	$\tau_2{}^{b,c}$ (ps)	a_3	$\tau_3{}^b$ (ps)	% missed
GlnRS	650	0.45	400	0.55	2000	−	−	64
GlnRS and $tRNA^{gln}$	650	0.25	450	0.75	2500	−	−	64
GlnRS and L-glutamine	750	0.35	750	0.65	2000	−	−	60
GlnRS, $tRNA^{gln}$, and L-glutamine	580	0.80	800	0.20	3250	−	−	67
GlnRS,[d] ATP, and $tRNA^{gln}$	520	0.43	100	0.47	350	0.10	2750	52
Y211H-GlnRS[d]	1080	0.37	150	0.47	1500	0.16	4350	42

[a] Within ±50 cm^{-1}. [b] Within ±10%. [c] $\langle\tau_s\rangle = a_1\tau_1 + a_2\tau_2$. [d] Fits best to a three-exponential fit.

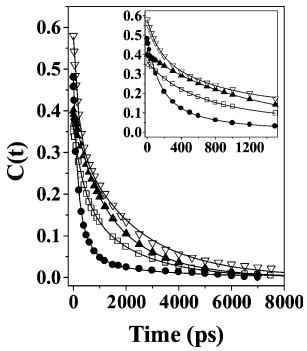

FIGURE 6: Decay of $C(t)$ of acrylodan-labeled (i) mutant Y211H-GlnRS (▽), (ii) GlnRS with glutamine (▲), (iii) wild-type GlnRS (□), and (iv) wild-type GlnRS with $tRNA^{gln}$ and ATP (●). The points denote the actual values of $C(t)$, and the solid lines denote the best fit to an exponential decay. The initial parts of the decays of $C(t)$ are shown in the inset.

where ν_{em}^{np} and ν_{abs}^{np} denote the steady-state frequencies of emission and absorption, respectively, of the probe in a nonpolar solvent. After binding to the sulfhydryl group, acrylodan (**I**) resembles 6-propionyl-2-(*N*,*N*-dimethylamino)-naphthalene (PRODAN, II, Scheme 1). Thus, we used absorption (342 nm) and emission (391 nm) maxima of PRODAN in *n*-heptane as the nonpolar solvent. Using eq 4, we found that for acrylodan-labeled GlnRS 64% of the total dynamic solvent shift is missed and only 36% of the total solvent shift is detected in our setup. Thus, as shown in Figure 6, in this case the decay of $C(t)$ starts from 0.36. Figure 6 and Table 1 summarize the decay parameters of $C(t)$ and also list the amount of solvation missed for various systems. For acrylodan-labeled GlnRS in the free state, the decay of $C(t)$ exhibits two components of approximately 400 and 2000 ps. In the case of a solvation probe (thioaminophthalimide, TAP) placed ≈3 Å from the surface of GlnRS, the solvation dynamics exhibits two components of 40 ps (85%) and 580 ps (15%) (*20*). It may noted that according to computer simulations solvation dynamics becomes faster with an increase in the distance from the protein surface and at a distance of >10 Å the dynamics is bulklike (*2*). Thus, the slower dynamics of acrylodan-labeled GlnRS compared to those of TAP-labeled GlnRS is ascribed to the location of acrylodan deeper inside the protein.

Solvation Dynamics of Acrylodan-Labeled Wild-Type GlnRS Bound to Glutamine, tRNA, and ATP. In this section, we will discuss the effect of binding of glutamine, $tRNA^{gln}$, and ATP to acrylodan-labeled GlnRS. Figure 6 and Table 1 summarize the decay characteristics of $C(t)$ of wild-type GlnRS bound to $tRNA^{gln}$, glutamine, and ATP.

Upon addition of cognate tRNA ($tRNA^{gln}$), fluorescence decays of acrylodan-labeled GlnRS become slightly slower. In this case, the decay at the blue end (440 nm) is described by two components of 830 and 4200 ps and the decay at the red end (590 nm) displays a decay with a time constant of 4500 ps and a rise component of 600 ps. It is readily seen that binding of tRNA affects the 2000 ps component of acrylodan-labeled GlnRS and lengthens it to 2500 ps while the 400 ps component remains unchanged. In this case, ~60% of the total solvation is missed (Figure 6 and Table 1).

As shown in Figure 6 and Table 1, when glutamine binds to GlnRS, the 400 ps component becomes longer (750 ps) while the 2000 ps component is unaffected. This suggests that at the active site of GlnRS there exist two kinds of water molecules, both much slower than bulk water (~1 ps). Glutamine binding affects the 400 ps component, while $tRNA^{gln}$ affects the 2000 ps component. When both glutamine and $tRNA^{gln}$ bind to GlnRS, the solvation dynamics exhibits two components of 750 and 3250 ps (Figure 6 and Table 1). Evidently, in this case, both the sites are occupied, and hence, both the 400 and 2000 ps components are modified.

Acrylodan-Labeled Mutant Protein Y211H-GlnRS. Since the active site of a multisubstrate enzyme like GlnRS spans a considerable distance, mutation of residues at the active site may shed further light on the localization of different classes of water molecules. According to the crystal structure of GlnRS, Y211 is present at the active site with several crystallographic water molecules bonded through the side chain hydroxyl group and is involved in substrate glutamine binding (Figures 1 and 2) (*35*, *36*). A site-directed mutant was constructed (Y211H) in which a conservative substitution was made by replacing tyrosine with histidine so that the tyrosine side chain hydroxyl group was absent. This mutant does not exhibit any catalytic activity and, hence, has a disrupted active site. This is expected as Y211 hydrogen bonds with the substrate (glutamine) and is a crucial residue involved in molecular recognition and catalysis.

Circular Dichroism and Acrylamide Quenching of Y211H-GlnRS. In the absence of catalytic activity, we have checked the integrity of the structure of the mutant protein by circular dichroism (CD) and fluorescence spectroscopy. Figure 7 shows the CD spectra of the wild type and Y211H-GlnRS. The two spectra are almost identical, indicating nativelike secondary structure in the mutant. Fluorescence properties of tryptophan are sensitive monitors of the conformation of proteins. GlnRS has eight tryptophans distributed throughout its structure. The emission maximum of the mutant protein was found to be very close to that of the wild-type protein. Acrylamide quenching is also used to monitor protein conformation and dynamics (Figure 8). The Stern−Volmer constant obtained from acrylamide quenching of tryptophan fluorescence is 4.6 ± 0.16 M^{-1}, which is very close to that obtained for the native protein, 5.04 ± 0.49 M^{-1} (*38*, *39*). The similarity between the CD spectra and acrylamide

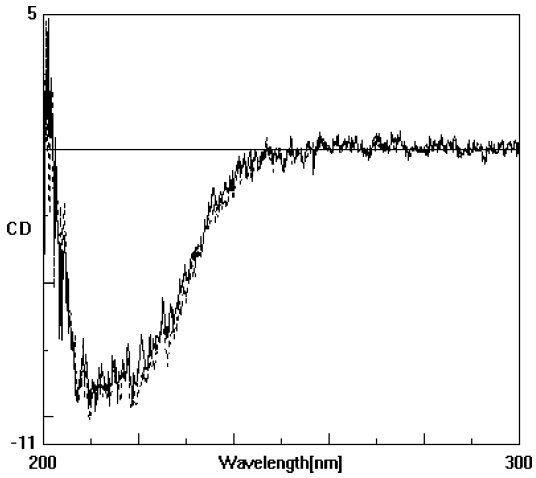

FIGURE 7: CD spectra of wild-type GlnRS (—) and Y211H-GlnRS (- - -). The concentrations of both proteins were kept at 2 μM. Solution conditions were 0.1 M Tris-HCl buffer (pH 7.5) containing 0.1 M KCl. The bandwidth was 1 nm.

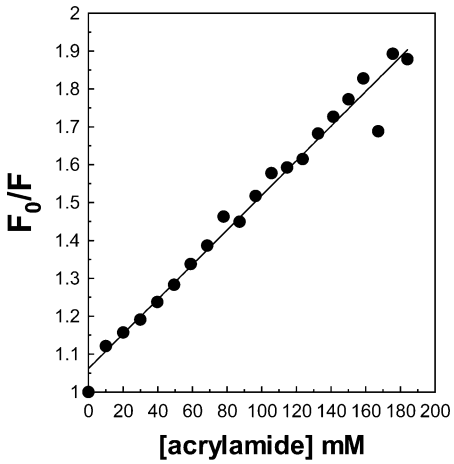

FIGURE 8: Stern−Volmer plot of acrylamide quenching of Y211H-GlnRS. The protein concentration was 2 μM in 0.1 M potassium phosphate buffer (pH 7.9) containing 0.1 M KCl and 0.1 mM EDTA. The excitation wavelength was 295 nm, and the emission wavelength was 341 nm. The band-pass was kept at 5 nm.

quenching of both the wild type and the biologically inactive mutant form of GlnRS suggests that these properties are not very sensitive indicators of the biological function. In the following section, we show that solvation dynamics in the wild-type and mutant forms are very different.

Solvation Dynamics of Y211H-GlnRS. Figure 6 includes decay of $C(t)$ as a function of time for the acrylodan-labeled mutant, Y211H. In this case, ~58% of the total decay is detected in our setup which is much larger than the amount (36%) detected for GlnRS. The shorter component of 400 ps in the case of GlnRS is substantially reduced to ~150 ps in Y211H, whereas the longer component is also reduced to ~1500 ps (Table 1). However, in addition, a substantially long component of 4350 ps was observed. It is apparent that all the classes of solvation dynamics are affected, indicating that the observed solvation dynamics originates from the active site.

Fluorescence Anisotropy Decay. The fluorescence anisotropy decays of acrylodan-labeled GlnRS in unligated form and with different ligands are described by a very fast component of ~40 ps (50%) and a very long component of

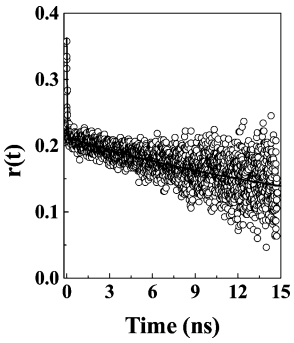

FIGURE 9: Fluorescence anisotropy decay, $r(t)$, of acrylodan-labeled GlnRS bound to glutamine and tRNA at an emission wavelength of 470 nm. The points (○) denote the actual values of $r(t)$, and the solid line denotes the best fit to a biexponential decay.

~20 ns (50%). A typical anisotropy decay is shown in Figure 9. It is evident that the components of anisotropy decays are very different from the components of decay of $C(t)$. One of the components of anisotropy decay (~40 ps) is much faster than the components of solvation dynamics (400 ps and 2 ns), and the other component of anisotropy decay (~20 ns) is much slower. Solvation dynamics is governed by the motion of the polar species (water molecules or polar residues). The anisotropy decay arises from the motion of the fluorescent probe with the motion of the macromolecular chain superimposed on it. The observed difference in the time scales of solvation dynamics and anisotropy decay suggests that solvation does not seem to originate from protein chain dynamics. However, one cannot rule out a contribution of segmental motion of the protein containing polar residues.

DISCUSSION

The most important findings of this work are as follows. First, this work demonstrates slow solvation dynamics (compared to that of bulk water) at the active site of GlnRS. Second, the components of solvation dynamics are found to be markedly affected upon binding of the substrates to the enzyme. Third, we show that the CD spectra and the acrylamide quenching of the protein in the wild-type and mutant (Y211H) forms are very similar. However, solvation dynamics in the free and mutant forms are very different. Fourth, we show that the time scales of solvent relaxation are very different from those of anisotropy decay.

We previously showed that the solvation dynamics of a covalent probe (TAP) residing at the surface of GlnRS and attached to the most reactive cysteine (C229) of GlnRS by a linker with a length of 3 Å reveal two components, 40 and 580 ps (*20*). In the case presented here, the probe (acrylodan) is directly attached to C229 and shows slower components (400 and 2000 ps) of solvation dynamics. Large-scale computer simulations indicate that the mobility of the water molecules is restricted at the protein surface but increases with distance from the protein surface (*2*). Thus, the slower solvation dynamics of acrylodan compared to that of TAP may be ascribed to the deeper location of acrylodan in the same protein. In other words, within a protein the solvation dynamics varies from site to site.

This work reveals that for free GlnRS the solvation dynamics at the active site exhibits two components of 400 and 2000 ps. When glutamine binds to GlnRS, the 400 ps

component is lengthened to 750 ps, keeping the 2000 ps component unaffected, while tRNA keeps the 400 ps component unchanged but lengthens the other to 2500 ps. When both glutamine and $tRNA^{gln}$ bind to GlnRS, both the 400 and 2000 ps components become longer. The major source of solvation dynamics is the motion of the polar species, namely, water molecules and the polar residues of the proteins. The presence of such a slowly relaxing solvation environment gives the active site a preorganized character on the time scale of 100−1000 ps. Since the hydrogen bond making and breaking in the catalytic cycle take place at a much faster rate (∼1 ps) (*25*, *44*−*46*) than this, the active site remains organized during the catalytic cycle. How enzymes enhance catalytic rates has been the subject of many investigations. A number of proposals have been espoused, including the role of entropy. Recently, however, much emphasis is being placed on the role of the preorganized active site. To our knowledge, we provide the first direct experimental evidence of a preorganized active site of an enzyme.

We have also attempted to clarify the role of water molecules in solvation dynamics. It has been observed that the dynamics of water molecules are distinctly slower in D_2O. In D_2O, the solvation dynamics of GlnRS labeled with acrylodan at C229 was found to be ∼30% slower (data not shown). This suggests water dynamics plays a major role in the solvation dynamics described here. However, motion of polar residues of the protein is also expected to play an important role, as well. Several recent works have included the motion of the polar residues by invoking the idea of polymer chain dynamics (Rouse chain dynamics) (*14*).

The relationship between dynamics and catalysis by an enzyme is still an unresolved question. Two major ideas have emerged in recent times. One is the preorganized active state, which implies that the active site of an enzyme is relatively static on the time scale of bond making or breaking (*3*), and the other is that motions of side chains are dynamically coupled to the motions of the substrate during catalytic turnover (*6*). Bond making and breaking probably occur on sub-picosecond time scales, suggesting that slow relaxations detected here would make active sites appear to be static during the bond making or breaking steps (preorganized). Time scales of motions of side chains observed by Eisenmesser et al. (*6*) are in the hundreds of microseconds, much slower than the solvent motion detected here. However, nanosecond time scale motions of water molecules associated with the active site probably imply far more rigid side chains. Thus, dynamical coupling of side chain motions on the longer time scale is not inconsistent with the results obtained here. The preorganization and implied static character are relevant during bond making and breaking which is much faster than the macroscopic observed rate constants which are combinations of unresolved microscopic steps, including residence times at a particular state.

Substrate selection is an important property of an enzyme. In aminoacyl-tRNA synthetases (aaRS), high specificity is of utmost importance as wrong substrate selection leads to a higher error rate in protein synthesis. The aaRSs have evolved several mechanisms for increasing specificity (*47*). In the subgroup of aaRS to which glutaminyl-tRNA synthetase belongs, the amino acid binding in proper mode and affinity is dependent upon prior binding of the cognate tRNA, ensuring that only the correct amino acid is loaded onto the correct tRNA. The anticodons of $tRNA^{gln}$ are important recognition elements, and mutation of anticodon bases led to a much reduced activity (*48*−*50*). A large component of this activity is a reduction of k_{cat}. Since the anticodon bases bind several tens of angstroms from the active site, it has been postulated that the binding of the anticodon creates a reordering of the active site by long distance conformational change (*36*). However, little evidence has been presented so far in support of this mechanism. In this article, we have demonstrated the existence of two slowly relaxing components of solvation dynamics at the active site of GlnRS: one with a relaxation time of 400 ps and the other with a relaxation time of 2000 ps. The slower solvation dynamics become even slower upon binding of $tRNA^{gln}$. This indicates a cognate tRNA-dependent reorganization of the active site and further ordering. The excess of crystallographic water molecules in the active site in the presence of substrates also supports the idea that the active site is more organized in the substrate-bound form (Figure 2). If the binding of correct substrates leads to proper preorganization (complementary to the transition state), correct substrate binding will lead to higher catalytic efficiency, thus enhancing specificity. Slow solvation dynamics at the active site, as revealed in this work, seems to be essential for molecular recognition by an enzyme.

REFERENCES

1. Simonson, T., Archontis, G., and Karplus, M. (2002) Free energy simulations come of age: Protein−ligand recognition, *Acc. Chem. Res. 35*, 430−437.
2. Makarov, V., Petit, B. M., and Feig, M. (2002) Solvation and hydration of proteins and nucleic acids: A theoretical view of simulation and experiment, *Acc. Chem. Res. 35*, 376−384.
3. Warshel, A. (2003) Computer simulations of enzyme catalysis: Methods, progress, and insights, *Annu. Rev. Biophys. Biomol. Struct. 32*, 425−443.
4. Jencks, W. P. (1997) From chemistry to biochemistry to catalysis to movement, *Annu. Rev. Biochem. 66*, 1−18.
5. Cannon, W. R., and Benkovic, S. J. (1998) Solvation, reorganization energy, and biological catalysis, *J. Biol. Chem. 273*, 26257−26260.
6. Eisenmesser, E. Z., Bosco, D. A., Akke, M., and Kern, D. (2002) Enzyme dynamics during catalysis, *Science 295*, 1520−1523.
7. Dellerue, S., and Bellisent-Funnel, M.-C. (2000) Relaxational dynamics of water molecules at protein surface, *Chem. Phys. 258*, 315−325.
8. Modig, K., Liepinsh, E., Otting, G., and Halle, B. (2004) Dynamics of protein and peptide hydration, *J. Am. Chem. Soc. 126*, 102−114.
9. Denisov, V. P., Jonsson, B.-H., and Halle, B. (1999) Hydration of denatured and molten globule proteins, *Nat. Struct. Biol. 6*, 253−260.
10. Jordanides, X. J., Lang, M. J., Song, X., and Fleming, G. R. (1999) Solvation dynamics in protein environments studied by photon echo spectroscopy, *J. Phys. Chem. B 103*, 7995−8005.
11. Lundgren, J. S., Heitz, M. P., and Bright, F. V. (1995) Dynamics of acrylodan-labeled bovine and human serum albumin sequestered within aerosol-OT reverse micelles, *Anal. Chem. 67*, 3775−3781.
12. Nandi, N., Bhattacharyya, K., and Bagchi, B. (2000) Dielectric relaxation and solvation dynamics of water in complex chemical and biological systems, *Chem. Rev. 100*, 2013−2046.
13. Bhattacharyya, K. (2003) Solvation dynamics and proton transfer in supramolecular assemblies, *Acc. Chem. Res. 36*, 95−101.
14. Pal, S. K., and Zewail, A. H. (2004) Dynamics of Water in Biological Recognition, *Chem. Rev. 104*, 2099−2124.
15. Changenet-Barret, P., Choma, C. T., Gooding, E. F., Degrado, W. F., and Hochstrasser, R. M. (2000) Ultrafast dielectric response of proteins from dynamic Stokes shifting of coumarin in calmodulin, *J. Phys. Chem. B 104*, 9322−9329.

16. Toptygin, D., Savichenko, R. S., Meadow, N. D., and Brand, L. (2001) Homogeneous spectrally- and time-resolved fluorescence emission from single-tryptophan mutants of IIA^{Glc} protein, *J. Phys. Chem. B 105*, 2043−2055.
17. Gearheart, L. A., Somoza, M. M., Rivers, W. E., Murphy, C. J., Coleman, R. S., and Berg, M. A. (2003) Sodium-ion binding to DNA: Detection by ultrafast time-resolved stokes-shift spectroscopy, *J. Am. Chem. Soc. 125*, 11812−11813.
18. Brauns, E. B., Madaras, M. L., Coleman, R. S., and Berg, M. (2002) Complex local dynamics in DNA on the picosecond and nanosecond time scales, *Phys. Rev. Lett. 88*, 158101-1-4.
19. Sen, P., Mukherjee, S., Dutta, P., Halder, A., Mandal, D., Banerjee, R., Roy, S., and Bhattacharyya, K. (2003) Solvation dynamics in the molten globule state of a protein, *J. Phys. Chem. B 107*, 14563−14568.
20. Mandal, D., Sen, S., Sukul, D., Bhattacharyya, K., Mandal, A. K., Banerjee, R., and Roy, S. (2002) Solvation dynamics of a probe covalently bound to a protein and in an AOT microemulsion: 4-(*N*-Bromoacetylamino)phthalimide, *J. Phys. Chem. B 106*, 10741−10747.
21. Dutta, P., Sen, P., Halder, A., Mukherjee, S., Sen, S., and Bhattacharyya, K. (2003) Solvation dynamics in a protein-surfactant complex, *Chem. Phys. Lett. 377*, 229−235.
22. Nandi, N., and Bagchi, B. (1997) Dielectric relaxation of biological water, *J. Phys. Chem. B 101*, 10954−10961.
23. Marchi, M., Sterpone, F., and Ceccarelli, M. (2002) Water rotational relaxation and diffusion in hydrated lysozyme, *J. Am. Chem. Soc. 124*, 6787−6791.
24. Sterpone, F., Ceccarelli, M., and Marchi, M. (2001) Dynamics of hydration in hen egg white lysozyme, *J. Mol. Biol. 311*, 409−419.
25. Balasubramanian, S., Pal, S., and Bagchi, B. (2002) Hydrogen bond dynamics near a miceller surface: Origin of the universal slow relaxation at complex aqueous interfaces, *Phys. Rev. Lett. 89*, 115505-1-4.
26. Pal, S., Balasubramanian, S., and Bagchi, B. (2003) Identity, energy, and environment of interfacial water molecules in a micellar solution, *J. Phys. Chem. B 107*, 5194−5202.
27. Bruce, C. D., Senapati, S., Berkowitz, M. L., Perera, L., and Forbes, M. D. E. (2002) Molecular dynamics simulations of sodium dodecyl sulfate micelle in water: The behavior of water, *J. Phys. Chem. B 106*, 10902−10907.
28. Faeder, J., Albert, M. V., and Ladanyi, B. M. (2003) Molecular dynamics simulations of the interior of aqueous reverse micelles: A comparison between sodium and potassium counterions, *Langmuir 19*, 2514−2520.
29. Senapati, S., and Chandra, A. (2001) Dielectric constant of water confined in a nanocavity, *J. Phys. Chem. B 105*, 5106−5109.
30. Michael, D., and Benjamin, I. (2001) Molecular dynamics computer simulations of solvation dynamics at liquid/liquid interfaces, *J. Chem. Phys. 114*, 2817−2824.
31. Fecko, C. J., Eaves, J. D., Loparo, J. J., Tokmakoff, A., and Geissler, P. L. (2003) Ultrafast hydrogen-bond dynamics in the infrared spectroscopy of water, *Science 301*, 1698−1702.
32. Jimenez, R., Fleming, G. R., Kumar, P. V., and Maroncelli, M. (1994) Femtosecond solvation dynamics of water, *Nature 369*, 471−473.
33. Nandi, N., Roy, S., and Bagchi, B. (1995) Ultrafast solvation dynamics in water: Isotope effects and comparison with experimental results, *J. Chem. Phys. 102*, 1390−1397.
34. Jarzeba, W., Walker, G. C., Johnson, A. E., Kahlow, M. A., and Barbara, P. F. (1988) Femtosecond microscopic solvation dynamics of aqueous solutions, *J. Phys. Chem. 92*, 7039−7041.
35. Sherlin, L. D., and Perona, J. J. (2003) tRNA-dependent active site assembly in a class I aminoacyl-tRNA synthetase, *Structure 11*, 591−603.
36. Rould, M. A., Perona, J. J., Soll, D., and Steitz, T. A. (1989) Structure of *E. coli* glutaminyl-tRNA synthetase complexed with $tRNA^{Gln}$ and ATP at 2.8 angstrom resolution, *Science 246*, 1135−1142.
37. Uter, N. T., and Perona, J. J. (2004) Long-range intramolecular signaling in a tRNA synthetase complex revealed by pre-steady-state kinetics, *Proc. Natl. Acad. Sci. U.S.A. 101*, 14396−14401.
38. Bhattacharyya, T., and Roy S. (1993) A fluorescence spectroscopic study of substrate-induced conformational changes in glutaminyl-tRNA synthetase, *Biochemistry 32*, 9268−9273.
39. Bhattacharyya, T., Bhattacharyya, A., and Roy, S. (1991) A fluorescence spectroscopic study of glutaminyl-tRNA synthetase from *Escherichia coli* and its implications for the enzyme mechanism, *Eur. J. Biochem. 200*, 739−745.
40. Aiyar, A., Xiang, Y., and Leis, J. (1996) Site-directed mutagenesis using overlap extension PCR, *Methods Mol. Biol. 57*, 177−191.
41. Lakowicz, J. R. (1999) *Principles of Fluorescence Spectroscopy*, Chapter 7, Kluwer/Plenum, New York.
42. Maroncelli, M., and Fleming, G. R. (1987) Picosecond solvation dynamics of coumarin 153: The importance of molecular aspects of solvation, *J. Chem. Phys. 86*, 6221−6239.
43. Fee, R. S., and Maroncelli, M. (1994) Estimating the time-zero spectrum in time-resolved emission measurements of solvation dynamics, *Chem. Phys. 183*, 235−247.
44. Kropman, M. F., and Bakker, H. J. (2001) Dynamics of water molecules in aqueous solvation shells, *Science 291*, 2118−2120.
45. Chandra, A. (2000) Effects of ion atmosphere on hydrogen-bond dynamics in aqueous electrolyte solutions, *Phys. Rev. Lett. 85*, 768−771.
46. Xu, H., and Berne, B. J. (2001) Hydrogen-bond kinetics in the solvation shell of a polypeptide, *J. Phys. Chem. B 105*, 11929−11932.
47. Reddy, G. B., Srinivas, V. R., Ahmad, N., and Surolia, A. (1999) Molten globule-like state of peanut lectin monomer retains its carbohydrate specificity. Implications in protein folding and legume lectin oligomerization, *J. Biol. Chem. 274*, 4500−4503.
48. Ibba, M., and Soll, D. (1999) Quality control mechanisms during translation, *Science 286*, 1893−1897.
49. Jahn, M., Rogers, M. J., and Soll, D. (1991) Anticodon and acceptor stem nucleotides in tRNA(Gln) are major recognition elements for *E. coli* glutaminyl-tRNA synthetase, *Nature 352*, 258−260.
50. Liu, J., Ibba, M., Hong, K.-W., and Soll, D. (1998) The terminal adenosine of $tRNA^{Gln}$ mediates tRNA-dependent amino acid recognition by glutaminyl-tRNA synthetase, *Biochemistry 37*, 9836−9842.

BI0473915